

## Diatoms control nutrient cycles in a temperate, wave-dominated estuary (southeast Australia)

Ralf R. Haese,<sup>1</sup> Emma J. Murray, Craig S. Smith, and Jodie Smith

Geoscience Australia, Marine and Coastal Environment Group, GPO Box 378, Canberra, 2601 Australian Capital Territory, Australia

Lesley Clementson

Commonwealth Scientific and Industrial Research Organization (CSIRO), Division for Marine and Atmospheric Research, GPO Box 1538, Hobart, Tasmania 7001, Australia

David T. Heggie

Geoscience Australia, Marine and Coastal Environment Group, GPO Box 378, Canberra, 2601 Australian Capital Territory, Australia

### Abstract

Diatoms are important primary producers within pelagic, benthic, and epiphytic communities, and their siliceous frustules sink rapidly to the sediment. We measured benthic nutrient and gas fluxes and water column and sediment properties in an estuary of southeastern Australia to identify control mechanisms coupling benthic and pelagic processes, in particular, how nutrients become fractionated by processes affecting benthic nutrient fluxes. During late spring, the water column of St. Georges Basin was oligotrophic, primary production was likely phosphorus (P) limited, and the phytoplankton community was dominated by cyanophytes. Molar ratios of dissolved inorganic carbon (TCO<sub>2</sub>) to silica (Si) benthic fluxes, however, were equal to the molar composition of diatoms, indicating that diatoms preferentially sink and deliver the most labile organic matter fraction to the sediment. The congruent release of Si and carbon (C) implies a coupling of processes mobilizing Si and C. Extracellular polymeric substances surrounding the siliceous frustule are the primary labile organic matter fraction, and their rate of mineralization limits the dissolution of the siliceous frustule. Because decomposing biomass in sediments leads to net di-nitrogen (N<sub>2</sub>) production and very efficient burial of P, the fate of diatoms significantly contributes to the removal of bioavailable nutrients. High dissolved inorganic nitrogen to dissolved inorganic P benthic flux ratios of 290 to 900 promote P limitation, particularly in shallow waterbodies with long water residence times.

Nutrient and carbon cycles in aquatic environments are inherently coupled to primary producers, because photosynthesis fixes dissolved nutrients and carbon into biomass, and the mineralization of biomass fuels dissolved nutrients back into the pool of bioavailable nutrients. The complexity of estuarine biogeochemical cycles arises from the vast range of interactions between different primary producers, microbial mineralization pathways, and physical–chemical conditions including hydrodynamics, light availability, and catchment-derived nutrient loads (Pedersen et al. 2004). Evidence for increasing nutrient levels, changes in biogeochemical pathways, and the ecological structure in

estuaries during historic time is abundant and can be related to enhanced land use, urbanization, and industrial discharge (e.g., Nixon 1995; Jørgensen and Richardson 1996; Smith et al. 2006). Despite significant progress in coastal and estuarine research aiming to understand, predict, and mitigate eutrophication for more than four decades, many critically important questions remain to be answered as a result of the complexity of interactions (Howarth et al. 2003).

Diatoms constitute important pelagic, benthic, and epiphytic primary producers, and each of the primary producer groups may dominate estuarine primary production at times and in particular regions. Tidal currents may force benthic diatoms to become frequently resuspended, enhancing primary production in the water column (Shaffer and Sullivan 1988), and once in suspension, benthic diatoms are likely to become redistributed within the estuary (Lucas 2003). Macrophytes not only provide substrate for epiphyton but they may affect production of microphytobenthos in two ways. Macrophytes reduce shear stress acting on the sediment surface; therefore, macrophytes reduce resuspension of benthic diatoms. But macrophytes also lower light availability at the sediment surface, counterbalancing the former positive effect (Lassen et al. 1997).

<sup>1</sup> Corresponding author (ralf.haese@ga.gov.au).

### Acknowledgments

The Shoalhaven City Council kindly provided bathymetry and catchment load data. We thank Ian Atkinson and Colin Tindall for their assistance in the field and for sample preparations. Kadija Oubelkheir (CSIRO, Division for Land and Water) is thanked for sampling and filtering water samples used for pigment analysis. Peter Harris and Perran Cook provided important comments on the manuscript. We are thankful for the detailed and constructive comments of the two anonymous reviewers.

This publication has received permission from the CEO of Geoscience Australia.

Benthic–pelagic coupling of silica (Si) is primarily related to diatoms. Diatoms have particularly high sinking rates as a result of their siliceous frustule and aggregation ('marine snow'). As a consequence, diatoms importantly contribute to the export of primary production to the ocean interior (Smetacek 1985) and may control new production in oceanic surface waters (Dugdale and Wilkerson 1998). More recently, diatom aggregates were also found to control the new production and carbon (C) flux to the sediment when the phytoplankton community was flagellate-dominated (Waite et al. 2005). Unlike the production of dissolved nitrogen (N) and phosphorus (P) by the microbial decomposition of organic matter, dissolved Si is produced by the (chemical) dissolution of the siliceous frustule. The respective dissolution rate was found to vary significantly between surface oceanic water and deep-sea sediments, a factor that has been attributed to differences in properties of the siliceous frustule and ambient physico-chemical conditions (Van Cappellen et al. 2002).

Multiple processes affect the benthic–pelagic exchange of N and P at the sediment surface. In the case of N, net benthic fluxes (into and out of the sediment) depend on the predominance of autotrophic or heterotrophic processes. N assimilation by microphytobenthos may extend to water depths of 15 m, but sediment net autotrophy may change to net heterotrophy at an intermediate depth (Sundbäck et al. 2004). Denitrification is closely coupled to N assimilation by microphytobenthos through two processes: (1) Under nitrate ( $\text{NO}_3^-$ )-rich bottom water conditions, microphytobenthos assimilates  $\text{NO}_3^-$ , and only a fraction of the net  $\text{NO}_3^-$  uptake is denitrified (Dalsgaard 2003); (2) Under  $\text{NO}_3^-$ -depleted bottom water conditions, coupled nitrification–denitrification in sediments is most effective in the absence of microphytobenthos, because microphytobenthos rapidly consumes available N, so that no net  $\text{NO}_3^-$  production is observed and denitrification rates are low (Risgaard-Petersen 2003). Oxygenated bottom water not only allows for coupled nitrification–denitrification to occur, but it also allows iron(oxy)hydroxide to form, which efficiently scavenges phosphate ( $\text{PO}_4^{3-}$ ) diffusing upward within the sediment and thereby limits the benthic P flux (Slomp et al. 1996).

In this study, we examine the mechanisms controlling the biomass flux to the sediment and the respective efficiency of sediments to mobilize, retain, and transform nutrients in an estuary with restricted water exchange with the ocean and relatively little freshwater inflow. Because of the long water residence time and relatively low catchment nutrient loads, benthic nutrient fluxes are expected to significantly affect nutrient ratios and availability in the water column. An enhanced understanding of estuarine nutrient dynamics will ultimately improve our capability to assess and mitigate coastal eutrophication.

## Materials and methods

*Study area and sample collection*—St. Georges Basin is located in New South Wales in southeastern Australia. It has a water surface area of 41 km<sup>2</sup> and a maximum water depth of 10 m, with 50% of the basin area being deeper

than 6 m (Fig. 1). The catchment has an area of 348 km<sup>2</sup>, of which 80% is forested. Presently, sediment, total N, and total P loads to St. Georges Basin are  $5.9 \times 10^6$ ,  $139 \times 10^3$ , and  $24 \times 10^3$  kg yr<sup>-1</sup>, respectively (Shoalhaven City Council pers. comm.). The sea grass area has declined from 3.75 to 3 km<sup>2</sup> during the past 40 yr (Meehan et al. 2005). A 7-km-long channel between the basin-shaped estuary and the ocean is continuously open and strongly restricts water exchange with the ocean. As a consequence, the basin mean spring tide is 3.5 cm, the monthly mean ocean exchange is  $9.22 \times 10^7$  m<sup>3</sup>, and the annual mean water residence time is 80 d. The estimated mean monthly rate of freshwater inflow is only about 11% ( $1 \times 10^7$  m<sup>3</sup>) of the mean monthly ocean exchange. Because riverine inflow and tidal exchange are low, St. Georges Basin is classified as a wave-dominated estuary, which is the most common type of estuary in New South Wales ([www.ozestuaries.org](http://www.ozestuaries.org)).

Two surveys were carried out in St. Georges Basin during late spring time: In November 2003, benthic  $\text{NH}_4^+$ , Si, total dissolved inorganic carbon ( $\text{TCO}_2$ ),  $\text{O}_2$ , and  $\text{N}_2$  fluxes were derived from benthic chamber incubations at sites 1 to 5 (Fig. 1), with five benthic chambers at each site. From the same sites three cores were taken for core incubations, one for pore-water studies and one to derive chlorophyll *a* (Chl *a*) inventories and porosities. In November 2004, benthic  $\text{NH}_4^+$ , Si,  $\text{TCO}_2$ ,  $\text{O}_2$ ,  $\text{N}_2$ , and  $\text{PO}_4^{3-}$  fluxes were studied at sites 6 to 8 with benthic chambers only. At sites 6 to 17 one sediment core and one surface-water sample (0.5-m water depth) were taken by push-corer and Niskin bottle, respectively; photosynthetically active radiation (PAR) was measured at water depth intervals of 50 cm using a LI-COR light meter (LI-250A) with an underwater quantum sensor (LI-192). Sediment Chl *a* and porosity were determined on core samples and dissolved nutrients and total suspended matter were analyzed from surface-water samples. Pigments were analyzed from surface-water samples from site 6 and from sites 8 to 15. Sites 1 (9.8-m water depth) and 8 (8.1 m) are referred to as deep benthic sites, whereas sites 2 (1.6 m), 3 (1.6 m), 4 (2.0 m), 5 (2.2 m), 6 (1.1 m), and 7 (1.5 m) are shallow-water sites (Fig. 1).

*Benthic flux incubations and calculations*—Benthic nutrient ( $\text{NO}_x$ ,  $\text{NH}_4^+$ ,  $\text{PO}_4^{3-}$ , Si) and gas ( $\text{O}_2$ ,  $\text{TCO}_2$ ,  $\text{N}_2$ ) fluxes were derived from in situ benthic chamber and ex situ core incubations. Five manually operated benthic chambers were deployed at the shallow sites 2, 3, 4, 5, 6, and 7, and three automatic benthic chambers were deployed at the deep benthic sites 1 and 8. A benthic site had an area of about 100 m<sup>2</sup>. Two of the five manual chambers were transparent and three were blackened; out of the three automatic benthic chambers, one was transparent. Transparent and blackened benthic chambers were deployed in parallel to reveal the possible influence of benthic photosynthesis on benthic fluxes. All benthic chambers have a diameter of 29 cm, and the height of the incubated water body is typically 20 cm. Benthic chambers were slowly lowered to the sediment on a rope, and they sank into the sediment by about 5–10 cm. With an opening in the chamber's lid and a central stirrer operating at 6 rpm,

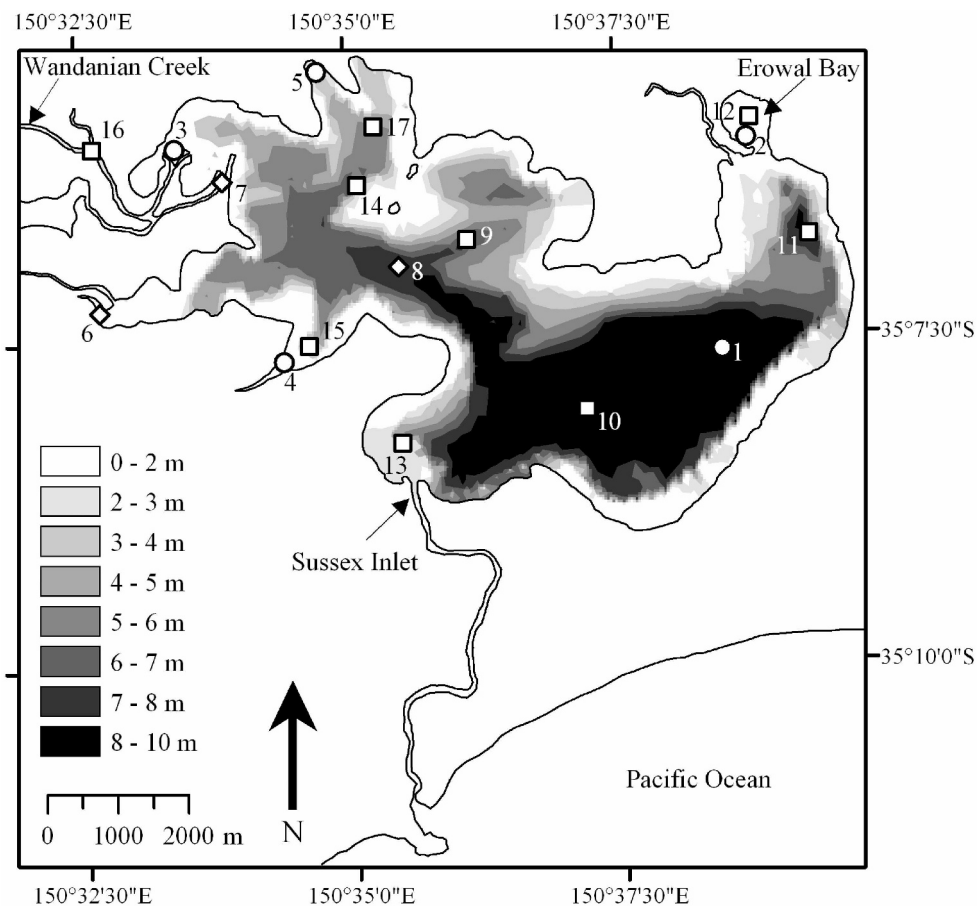


Fig. 1. Map of St. Georges Basin showing the bathymetry and sampling sites. Circles: benthic chamber sites. Squares: water column sites. Diamonds: combined benthic chamber and water column sites. Wandanian Creek is the major tributary entering the estuary at sites 3 and 7. Sussex Inlet is a 7-km-long channel that maintains water exchange between St. Georges Basin and the ocean. Sites 2 and 12 are located in Erowal Bay, a shallow embayment separated from a main basin by an inundated sandbar.

each chamber was equilibrated overnight before the incubation was begun, between 07:30 h and 08:30 h in the morning, by closing the lid. Self-logging probes (YSI) continuously measured salinity, temperature, and oxygen inside and outside of the chambers. Six chamber-water samples with a volume of 110 mL were taken over an incubation period of about 8 h, and one external sample was taken for reference. Once samples became available they were immediately filtered (0.45- $\mu$ m pore diameter) and split into subsamples for alkalinity, nutrient ( $\text{NO}_x$ ,  $\text{NH}_4^+$ ,  $\text{PO}_4^{3-}$ , Si), and  $\text{N}_2$  analysis. An unfiltered sample was taken for pH. All samples except for the nutrient sample had no headspace and were gas tight. Fifty microliters of concentrated  $\text{HgCl}_2$  solution was added to each 10-mL  $\text{N}_2$  sample. Nutrient analyses ( $\text{NH}_4^+$ , Si) were carried out in the field during the survey in 2003, and all nutrient samples from the 2004 survey were frozen before analysis ( $\text{NO}_x$ ,  $\text{NH}_4^+$ ,  $\text{PO}_4^{3-}$ , Si) in the New South Wales (NSW) Environment and Conservation laboratory.

Within each benthic site three cores with a typical sediment height of 30 cm and a water height of 20–30 cm were taken by pole corer for core incubations during the

2003 survey (sites 1–5). Cores had an inner diameter of 7.3 cm and were incubated for 8–10 h with a stirrer velocity of 6 rpm, under dark conditions and at in situ temperature (20–21°C). After 1 h of equilibration time and at the end of the incubation, the  $\text{O}_2$  concentration was measured by electrode (YSI), and water samples were taken for nutrient, alkalinity, and pH analysis. Water samples were treated as described for benthic chamber samples.

Benthic nutrient and gas fluxes were calculated from concentration changes over time by accounting for the incubated area and water volume. Changes in concentrations were corrected for the replenishment of sample volumes taken during benthic chamber incubations by ambient bottom water. Water incubated by benthic chambers and core incubations never reached oxygen concentrations below 20% saturation.

*Sediment sampling and treatment*—Cores with an inner diameter of 7.3 cm and a length of 30–40 cm were taken by pole corer, the bottom of the barrel was sealed with an O-ring fitted plug, and the top was closed off during transport with a rubber stopper. Within a few hours after core

retrieval, sediment from distinct depth intervals (0–0.5, 0.5–1, 1–1.5, 1.5–2, 2–2.5, 2.5–3, 3–4, 4–5, 5–6, 6–8, 8–10, and 10–12 cm) was extruded and subsampled for pore-water extraction, Chl *a* extraction, and porosity determination. Pore water was extracted by centrifugation (18,000 g, 10 min), and supernatant water was filtered (0.45- $\mu$ m pore size) and subsampled for TCO<sub>2</sub> and nutrient analysis. TCO<sub>2</sub> samples were kept gas-tight without headspace at room temperature for up to 1 d before analysis, while nutrient samples were kept frozen for up to 3 weeks before analysis. Chl *a* was extracted from sediment by weighing in 3–5 g of wet sediment, followed by addition of 10 mL of acetone (90%, saturated with MgCO<sub>3</sub>) and rigorous mixing on a vortex mixer, followed by placement in an ultrasonic bath for 30 min under dark conditions. The extraction solution was centrifuged and the acetone extract decanted and maintained at –10°C before analysis the next day. Porosity was determined from loss of water by drying the wet sediment at 60°C for 24 h.

*Analytical techniques*—For all benthic chamber and core incubation samples the alkalinity was determined by Gran titration, while the carbonate alkalinity was estimated by subtracting the alkalinity contribution of B(OH)<sub>4</sub><sup>–</sup>. TCO<sub>2</sub> was estimated from pH and carbonate alkalinity according to the method of Mehrbach et al. (1973). TCO<sub>2</sub> in pore waters was analyzed by means of conductivity in a basic receiving stream after the CO<sub>2</sub> had transferred from the acidified sample stream through a gas-permeable membrane (Hall and Aller 1992).

Dissolved nutrients (NH<sub>4</sub><sup>+</sup>, NO<sub>x</sub>, PO<sub>4</sub><sup>3–</sup>, Si) were determined by continuous flow analysis using a Bran+Luebbe (B+L) Auto Analyser 3. The analyses were based on standard colorimetric methods (Grasshoff et al. 1983).

N<sub>2</sub> analysis was carried out at Southern Cross University Environmental Analysis Laboratory according to the methods of Kana et al. (1994), but with the following modifications: Gases were detected with a Balzers QMS422 quadrupole mass spectrometer, and a water bath ( $\pm$ 0.01°C) was used to stabilize sample temperature in the water line upstream of the membrane. The effect of O<sub>2</sub> in the sample on the N<sub>2</sub> signal measured by the membrane inlet mass spectrometer was corrected by making a standard curve of O<sub>2</sub> concentration against N<sub>2</sub>:argon (Ar) ratios using water standards made from the incubation water equilibrated with the atmosphere at constant temperature (Eyre et al. 2002).

Chl *a* concentration in sediment extracts was calculated from spectrophotometric readings at wavelengths of 664 nm and 750 nm without and with the addition of 0.1 mol L<sup>–1</sup> HCl using the equation derived by Lorenzen (1967).

Total organic carbon (TOC) and total nitrogen (TN) were analyzed from the uppermost sediment slice (0–0.5 cm) after the samples were pretreated with acid and washed with demineralized water to remove carbonate and residual acid. TOC and TN were analyzed using an elemental analyzer (EA) attached to an isotope ratio mass spectrometer (Fry et al. 1992). At Geoscience Australia, a Thermo Finnigan Flash EA is coupled to a Finnigan Mat 252. The oxidation furnace of the Flash EA was packed with copper oxide and silvered

cobaltous oxide and operated at 900°C. The reduction furnace was packed with pure copper and operated at 600°C. Combustion products were separated on a packed GC column run isothermally at 40°C. We conducted carbon and nitrogen analysis separately to improve analytical performance. The precision of sample analysis was better than 10% for TOC and better than 5% for TN.

Pigments were analyzed from filtered surface-water samples. Approximately 1 liter of surface water was filtered through a 47-mm GF filter (Whatman) on the day of sampling and stored in liquid nitrogen until analysis. Filter samples were extracted in 100% acetone, vortexed for 30 s, sonicated in an ice-water bath for 15 min in the dark, and then kept in the dark at 4°C for approximately 15 h. After this time, 200  $\mu$ L of water was added to the acetone such that the final extract mixture was 90:10 acetone:water (vol:vol) and was sonicated once more in an ice-water bath for 15 min. The extracts were quantitatively transferred to a clean centrifuge tube and centrifuged to remove the filter paper. The final extract was filtered through a 0.2- $\mu$ m membrane filter (Whatman, anatope) prior to analysis. Pigment analysis was carried out using a Waters–Alliance high-performance liquid chromatography system, comprising a 2695XE separations module with column heater and refrigerated autosampler and a 2996 photo-diode array detector. Sample extract was mixed with a buffer solution (90:10 28 mmol L<sup>–1</sup> tetrabutyl ammonium acetate (pH 6.5):methanol) within the sample loop, and pigments were separated using a Zorbax Eclipse XDB-C8 stainless-steel 150  $\times$  4.6-mm-internal diameter column with 3.5- $\mu$ m particle size (Agilent Technologies) and a gradient elution procedure with solvent A (70:30 28 mmol L<sup>–1</sup> tetrabutyl ammonium acetate (pH 6.5):methanol) and solvent B (100% methanol). The flow rate was 1.1 mL min<sup>–1</sup> and the column temperature was 55°C. The separated pigments were detected at 436 nm and were identified against standard spectra using Waters Empower software. Pigment concentrations were determined from commercial and international standards (Sigma).

A set of diagnostic pigments (Jeffrey and Vesik 1997; Jeffrey and Wright 2006) are used for semiquantitative estimates of algal classes in this study. The abundance of these diagnostic pigments provide a simplified guide to the composition of a phytoplankton community, including identifying classes of small flagellates that cannot be determined by light microscopy techniques. In this study the presence of fucoxanthin has been used to indicate diatoms; peridinin—dinoflagellates; 19'-hexanoyloxyfucoxanthin (hex-fuco)—haptophytes; alloxanthin—cryptophytes; prasinoloxanthin—prasinophytes; zeaxanthin—cyanophytes and chlorophyll *b* (Chl *b*)—chlorophytes and green algae.

Total P (TP) was determined as part of the analysis of major elements in sediments by X-ray fluorescence according to a modified version of Norrish and Hutton's (1969) method and using a Philips PW2404 4kW sequential spectrometer. The instrument was calibrated using United States Geological Survey (USGS) and South African Reference Material international standards. The reported precision was better than 5%.

**Calculations**—The light attenuation coefficient,  $K_d$ , is calculated from the PAR profiles using the Bouguer–Lambert Law:  $K_d = \ln(I_0/I_z)/z$ .  $I_0$  is light intensity at the water surface and  $I_z$  is light intensity at depth  $z$  (e.g., Kirk 1994).

Excess Chl  $a$  (= total – background) concentration per volume of wet sediment was calculated for each depth interval in a core (*see above*) by accounting for the porosity and by assuming a particle density of  $2.65 \text{ g cm}^{-3}$ . The minimum Chl  $a$  concentration within the top 12 cm of a core was used as background concentration. The sediment Chl  $a$  inventory was then calculated as the sum of excess Chl  $a$  in each interval divided by the length of the studied section. The flux of Chl  $a$  and respective organic carbon to the sediment,  $J$ , was calculated assuming a quantitative balance between Chl  $a$  supply and breakdown (Sun et al. 1994):  $J = \lambda \times I$ , where  $\lambda$  is the decay constant and  $I$  the Chl  $a$  inventory. The assumption of steady state between the depositional flux and breakdown is reasonable, because Chl  $a$  monitoring data show very little interannual and intra-annual variability (Shoalhaven City Council unpubl. data). The temperature-dependent decay constant was derived from previous work (Sun et al. 1993) (i.e., for the given water temperature of  $21^\circ\text{C}$ ,  $\lambda$  is  $0.075 \text{ d}^{-1}$ ). In order to estimate the organic carbon flux to the sediment, a C:Chl  $a$  (wt:wt) ratio range of between 50 and 75 is used, as in previous studies (Boon and Duineveld 1998; Hagy et al. 2005).

Depth-dependant production rates per volume sediment,  $R$ , of  $\text{TCO}_2$  and Si are derived assuming zero-order kinetics, constant porosity, and steady state (Vanderborght and Billen 1975).  $R$  is in balance with the consumption of a solute because of diffusion away from the location of production,  $R = D_s d^2 C/dz^2$ , with  $C$  being the concentration and  $z$  the depth. The effective diffusion coefficient in the sediment,  $D_s$ , was derived according to standard procedures (e.g., Schulz 2006). A second-order polynomial fit,  $C = az^2 + bz + z$ , is derived for convex-shaped pore-water concentration profile intervals, and the constant  $a$  is used to solve for  $R$  in  $R = D_s \times 2a \times \phi$ , with  $\phi$  being the porosity. The top sediment interval (0–0.5 cm) was not included when deriving  $R$ , because concentration gradients may significantly steepen in oxic surface sediments (*see Discussion*), which is not detectable with the given sample resolution.

In a second step, production rates in the top sediment interval (0–0.5 cm) were calculated from the difference between the average total benthic flux derived by benthic chambers and the depth-integrated production rates below 0.5 cm. Because the calculated production rates derived from pore-water profiles do not account for bioirrigation, depth-integrated production rates are multiplied with a bioenhanced flux factor of 5. The latter is estimated based on previous studies (Berelson et al. 1998; Forster et al. 1999).

## Results

**Water column**—Surface-water properties studied during late spring (November) of 2004 reveal a spatially consistent pattern: Except for the brackish sites 16 and 7 upstream

and at the mouth of Wandanian Creek, respectively, salinities vary between 32 and 33.2 (Table 1), which reflects the predominant inflow of seawater relative to freshwater and good mixing throughout the basin. Surface-water temperatures were between  $20^\circ\text{C}$  and  $22^\circ\text{C}$  in the main basin and  $24^\circ\text{C}$  in Erowal Bay (site 12). Very similar salinity and temperature conditions were found during the November 2003 survey (data not shown). The shallowest sites (6 and 12) have a water depth of about 1 m and show the highest total suspended matter concentrations in surface waters. Chl  $a$  concentrations are very homogeneous throughout the basin, with concentrations ranging between  $1.9$  and  $2.7 \mu\text{g L}^{-1}$ . Similarly, light attenuation coefficients vary little throughout the main basin ( $0.41$ – $0.73 \text{ m}^{-1}$ ), but significantly higher values are recorded at the brackish sites 16 and 7, as well as in Erowal Bay (site 12). The average PAR per day at the bottom of each site (Table 1) shows that sites at water depths between 1 m and 2.5 m receive an average light flux that is larger than  $90 \mu\text{mol m}^{-2} \text{ s}^{-1}$ , whereas sites at water depths greater than 3.5 m only receive less than  $30 \mu\text{mol m}^{-2} \text{ s}^{-1}$ .

Dissolved nutrient concentrations in the main basin vary little for  $\text{NO}_x$  ( $0.31$ – $0.46 \mu\text{mol L}^{-1}$ ),  $\text{PO}_4^{3-}$  ( $0.02$ – $0.04 \mu\text{mol L}^{-1}$ ), and Si ( $36.8$ – $45.4 \mu\text{mol L}^{-1}$ ), while  $\text{NH}_4^+$  varies between  $0.3$  and  $7.4 \mu\text{mol L}^{-1}$  (Table 1). The highest  $\text{NH}_4^+$  concentrations are found at the shallow ( $\sim 1$ -m) sites 6 and 12. The brackish sites 16 and 7 have significantly higher  $\text{NO}_x$  ( $\sim 1.5$ - $\mu\text{mol L}^{-1}$ ) and lower Si ( $\sim 27$ - $\mu\text{mol L}^{-1}$ ) concentrations. Ratios of dissolved inorganic nitrogen (DIN) to dissolved inorganic phosphorous (DIP) generally exceed the Redfield ratio of 16 as a result of consistently very low  $\text{PO}_4^{3-}$  concentrations and relatively high  $\text{NH}_4^+$  concentrations.

**Pigments**—The distribution of diagnostic pigments follows the distribution of physical–chemical properties in the surface water (i.e., all sites show a very similar pattern except for site 12, Erowal Bay; Fig. 2). At all sites within the main basin, zeaxanthin is the most abundant diagnostic pigment, followed by Chl  $b$ , fucoxanthin, prasinoxanthin, and hex-fuco. Peridinin and alloxanthin are the least abundant indicative biomarkers found in the main basin. At Erowal Bay (site 12), however, fucoxanthin by far exceeds other diagnostic pigments (Fig. 2). From a review of algal classes and their taxonomically significant pigments (Jeffrey and Vesik 1997) it is concluded that cyanophyta are predominant in the main basin given the very high abundance of zeaxanthin, followed by blue–green algae such as chlorophyta and prasinophyta, based on the abundances of Chl  $b$  and prasinoxanthin. Diatoms (bacillariophyta) constitute a minor fraction of total phytoplankton community in the main basin, but they are predominant in Erowal Bay (site 12) based on the abundances of fucoxanthin. Dinoflagellates (dinophyta), cryptophyta, haptophyta, and chrysophyta are quantitatively only of subordinate importance at all sites given the low abundances of peridinin, alloxanthin, and hex-fuco

**Benthic fluxes**—Figure 3 compares benthic fluxes measured in (1) core incubations under dark and in situ

Table 1. Surface-water properties at study sites (see Fig. 1). Chlorophyll *a*, Chl *a*; TSM, total suspended matter; Kd, light attenuation coefficient; DIN:DIP, ratio of dissolved inorganic nitrogen to dissolved inorganic phosphorous; Si, silica. The average photoactive radiation per day at the bottom, av. PAR<sub>bottom</sub>, is calculated using given daily solar radiation ( $15 \times 10^6 \text{ J d}^{-1}$ ), a factor of 4.4 to convert radiation to photon flux, and assuming 45% of solar radiation is PAR (Kirk 1994).

Site	Water depth (m)	Salinity ( $\mu\text{g L}^{-1}$ )	Chl <i>a</i> ( $\mu\text{g L}^{-1}$ )	TSM (mg L <sup>-1</sup> )	NH <sub>4</sub> <sup>+</sup> ( $\mu\text{mol L}^{-1}$ )	NOX ( $\mu\text{mol L}^{-1}$ )	PO <sub>4</sub> <sup>3-</sup> ( $\mu\text{mol L}^{-1}$ )	DIN:DIP	Si ( $\mu\text{mol L}^{-1}$ )	Kd (m <sup>-1</sup> )	av. PAR <sub>bottom</sub> ( $\mu\text{mol m}^{-2} \text{ s}^{-1}$ )
12	0.9	32.0	1.4	16.4	7.36	0.48	0.03	242.2	47.8	0.96	146
6	1.1	32.7	1.2	17.8	3.05	0.38	0.03	122.3	45.4	0.73	155
7	1.5	26.6	1.1	9.6	3.54	1.51	0.01	423.5	26.5	0.86	95
13	2.5	32.9	1.2	9.6	0.42	0.31	0.03	28.7	36.8	0.53	92
16	3.5	18.0	0.9	6.5	3.45	1.46	0.01	474.4	27.3	0.98	11
15	4.7	33.3	1.2	9.3	1.70	0.39	0.04	52.4	44.9	0.58	23
14	5	32.7	1.7	9.9	0.30	0.35	0.03	19.3	43.9	0.52	26
17	5.7	32.7	1.4	7.9	1.32	0.46	0.04	44.9	45.3	0.58	13
8	8.1	32.7	1.5	8.9	0.31	0.32	0.02	25.8	44.4	0.55	4
9	8.1	32.6	1.6	9.5	0.82	0.35	0.03	40.1	45.2	0.61	3
11	8.4	32.8	1.4	10.3	1.29	0.50	0.02	83.0	43.4	0.47	7
10	9	32.8	2.1	9.1	0.30	0.27	0.02	23.6	43.6	0.41	8

temperature conditions, (2) dark benthic chambers, and (3) transparent benthic chambers. For the deep sites 1 and 8 no discernable difference is observed between dark and light chambers, because the sediments are considered to be dark at all times, given average PAR photon fluxes per day of  $<10 \mu\text{mol m}^{-2} \text{ s}^{-1}$  (Table 1). All sites are net heterotrophic, as shown by the consistent flux of O<sub>2</sub> into and TCO<sub>2</sub> out of the sediment. However, significant differences in fluxes measured by the dark and transparent benthic chambers at the shallowest site 6 ( $\sim 1$  m), as well as at sites 4 and 5 ( $\sim 2$  m), indicate benthic photosynthesis by microphytobenthos under light conditions. Despite their shallow water depths ( $\sim 1.5$  m), sites 2, 3, and 7 do not show discernable differences in fluxes under transparent and dark conditions. The large spatial heterogeneity of microphytobenthos is often observed and can be caused by local differences in resuspension or grazing (Underwood and Kromkamp 1999). PO<sub>4</sub><sup>3-</sup> fluxes are very low (e.g., three orders of magnitude lower than NH<sub>4</sub><sup>+</sup> and Si fluxes), and PO<sub>4</sub><sup>3-</sup> fluxes appear not to be affected by differences in light availability.

Variability of fluxes within one benthic site ( $\sim 100 \text{ m}^2$ ) is generally very high, as shown by the high deviation from the average benthic flux in core incubations and in benthic chambers (Fig. 3). Despite this high variability, the deep sites 1 and 8 show the lowest of all fluxes. The comparison of dark benthic chamber and core incubation fluxes reveals a consistent offset in the magnitude of fluxes. Benthic fluxes derived by core incubations are consistently a factor of 2 to 3 lower than benthic chamber fluxes.

Ratios of benthic fluxes under dark conditions are presented in Fig. 4. Ratios of average benthic TCO<sub>2</sub> to Si fluxes per site are aligned very close along the 'diatom line' (Fig. 4a), which represents the molar ratio of TCO<sub>2</sub> to Si of 106:17 (6.2 C:1 Si) found in diatoms (Brezezinski 1985). Note that this consistency in the flux ratio is found in benthic chambers as well as in core incubations regardless of the offset in absolute fluxes found for the two approaches. Similarly, the benthic flux ratios between TCO<sub>2</sub> to NH<sub>4</sub><sup>+</sup> in benthic chambers and in core incubations are fairly constant (Fig. 4b). In this case, all data are close to a ratio of 11 TCO<sub>2</sub>:1 NH<sub>4</sub><sup>+</sup>, which is significantly higher than the Redfield ratio of 106:16 (6.6 C:1 N) (Redfield et al. 1963). A C:N ratio of 6.6 is expected for benthic fluxes, if the original marine biomass decomposes without preferential mobilization of one constituent and without secondary reactions affecting one or another constituent.

*TCO<sub>2</sub> and Si in pore waters and modelled production rates*—TCO<sub>2</sub> and Si pore-water profiles are convex-shaped, with the steepest concentration gradients at the sediment surface and reaching maximum concentrations asymptotically at depth (Fig. 5). Except for site 1, TCO<sub>2</sub> and Si profiles have very similar depth intervals where distinct curvatures are found. Site 1 is characterized by a large interval with a low rate of TCO<sub>2</sub> production ( $0.35 \text{ nmol cm}^{-3} \text{ h}^{-1}$ ), whereas the other sites reveal shorter depth intervals below a depth of 0.5 cm with higher TCO<sub>2</sub> and Si production rates (1–12 and 0.1–0.7  $\text{nmol cm}^{-3} \text{ h}^{-1}$ , re-

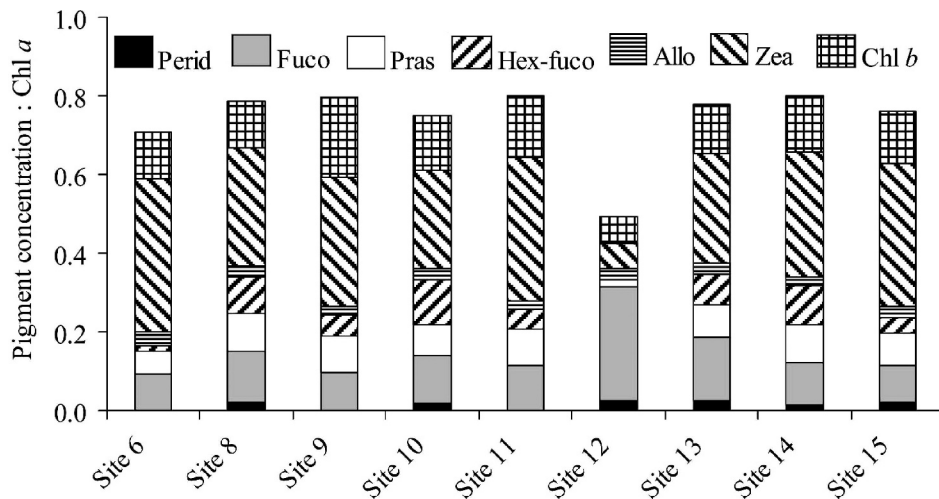


Fig. 2. Ratios of indicative pigments and chlorophyll *a* (Chl *a*). Full list of abbreviations, as follows: Perid, peridinin; Fuco, fucoxanthin; Pras, prasinoxanthin; Hex-fuco, 19-hexanoyloxyfucoxanthin; Allo, alloxanthin; Zea, zeaxanthin; Chl *b*, chlorophyll *b*. Pigment ratios are consistent throughout the main basin, where zeaxanthin : Chl *a* dominates. Fucoxanthin : Chl *a* dominates in Erowal Bay.

spectively). Interestingly,  $\text{TCO}_2$  and Si production rates in the top sediment interval (0–0.5 cm) are typically one order of magnitude higher than in the interval below, and  $\text{TCO}_2$ :Si production rate ratios in the top sediment interval are very close to the average molar C:Si ratio found in diatoms (Table 2). Note that the presented production rates do not account for bioirrigation; however, depth-integrated production rates multiplied with a bioenhanced flux factor of 5 match total benthic fluxes (see *Materials and methods: Calculations*).

*Chl a, TOC, TN, and TP concentrations in sediments*—Most down-core Chl *a* profiles exhibit maximum Chl *a* concentrations at the surface and a decrease with depth (Fig. 6). However, a high variability of Chl *a* concentrations at the sediment surface between sites and multiple subsurface maxima are found. Note also that the background Chl *a* concentrations are also highly variable. Chl *a* inventories and the respective organic C depositional fluxes vary by a factor of 5 throughout St. Georges Basin (Table 3).

TOC and TN concentrations in surface sediments vary greatly between 1.09 to 10.46 and 0.03 and 0.9 wt%, respectively (Table 3). Both variables correlate exponentially with porosity, and C:N ratios are distinctively higher at sites with low porosity (e.g., C:N ratios at sites 7 and 6 are 42 and 21, respectively, whereas C:N ratios at all other sites vary between 12 and 16). TP depth profiles typically show an enrichment in surface sediments, which gradually decrease asymptotically with depth (Fig. 7). The surface sediment enrichment in P is a first indication for P retention and limited P release back into the water column. Background values are found below ~10-cm depth and are typically ~0.06 wt%.

## Discussion

*Magnitude of benthic fluxes*—In this study we find two- to threefold higher in situ benthic fluxes for  $\text{O}_2$ ,  $\text{TCO}_2$ ,  $\text{NH}_4^+$ , and Si measured by benthic chambers as compared to ex situ core incubation fluxes, which agrees with similar observations presented elsewhere (Glud et al. 2003; Hammond et al. 2004). Increasing evidence argues for the need to represent macrofaunal activity at an appropriate spatial scale, because benthic fluxes are highly patchy on a centimeter to decimeter scale depending on the distribution of open burrows (Glud et al. 2003; Wenzhöfer and Glud 2004). Given the small area covered in core incubations (42 cm<sup>2</sup>) in comparison to benthic chambers (660 cm<sup>2</sup>) used in this study it is likely that there is an insufficient spatial representation of fauna activity in core incubations, which leads to a significant underestimate in benthic fluxes. Flux ratios derived by core incubations, however, appear not to be affected by the small incubation area, as  $\text{TCO}_2$ :Si and  $\text{TCO}_2$ : $\text{NH}_4^+$  ratios are indistinguishable between core and benthic chamber incubations (Fig. 4a,b). This observation indicates a constant ratio of bioenhanced solute fluxes regardless of the magnitude of the bioenhanced flux.

Measured N–N<sub>2</sub> fluxes reflect the net N<sub>2</sub> production in sediments and can be used to assess the capacity to transform DIN species into N<sub>2</sub>. A recent review of processes leading to N<sub>2</sub> production in sediments is provided by Hulth et al. (2005). It turns out that average dark N–N<sub>2</sub> fluxes are relatively constant ( $1.1 \pm 0.9 \text{ mmol m}^{-2} \text{ d}^{-1}$ ) regardless of the magnitude of  $\text{TCO}_2$  fluxes or ambient conditions, such as water depth (Fig. 3). As  $\text{NH}_4^+$  fluxes are highly variable, net N<sub>2</sub> production efficiencies based on measured N fluxes ( $= \text{N–N}_2 / [\text{NH}_4^+ + \text{N–N}_2] \times 100$ ) are

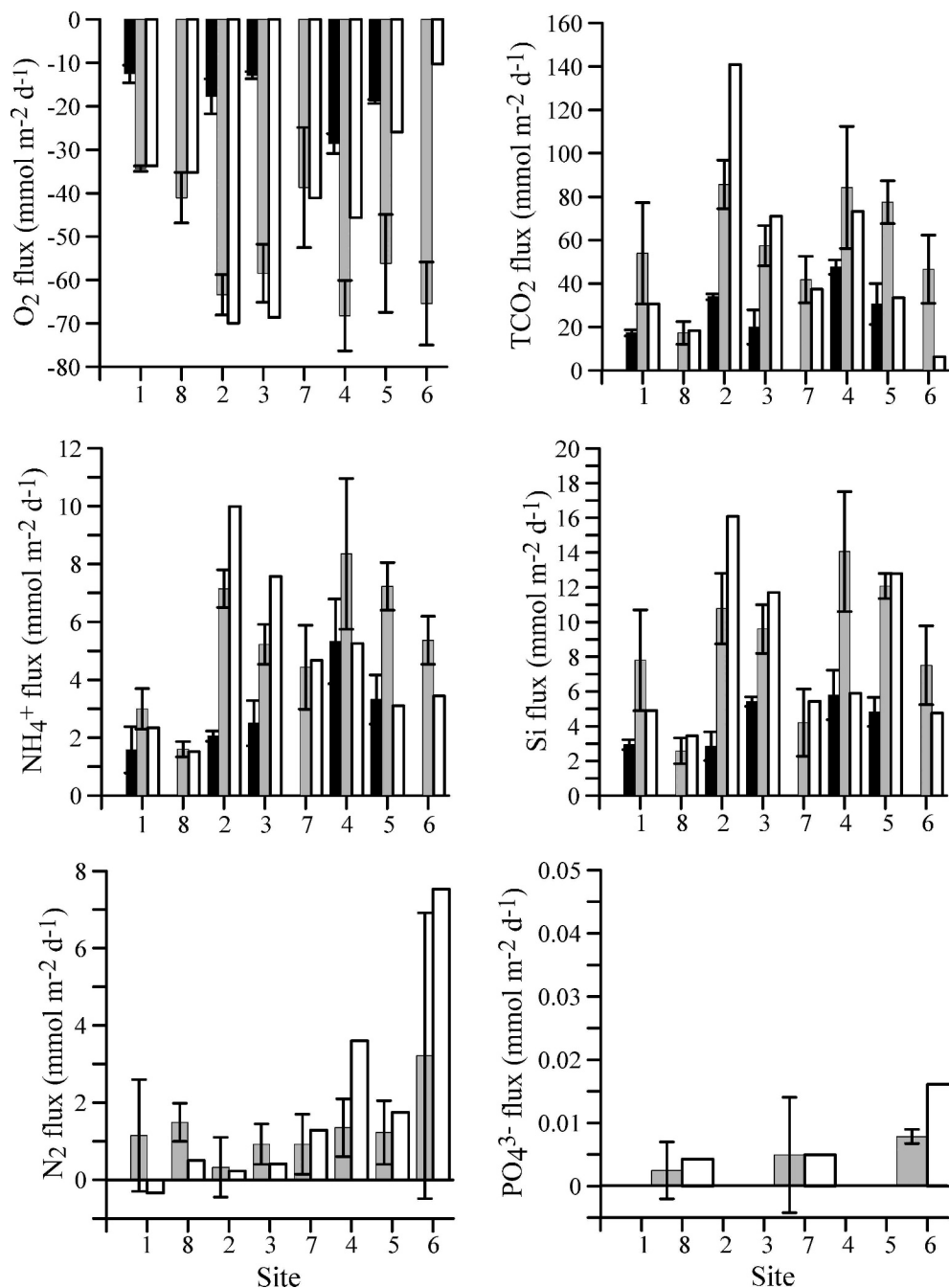


Fig. 3. Benthic nutrient ( $\text{NH}_4^+$ , Si,  $\text{PO}_4^{3-}$ ) and gas ( $\text{O}_2$ ,  $\text{TCO}_2$ ,  $\text{N}_2$ ) fluxes. Closed bar: average flux derived from core incubations in the laboratory under in situ temperatures and in darkness ( $n = 3$ ); gray bar: average flux derived from in situ benthic chamber incubations in darkness ( $n = 4$ ); open bar: flux derived from in situ benthic chamber incubation under natural light conditions ( $n = 1$ ). Error bars represent the deviation from the average. Sites 1 and 8 are at water depths of  $>8$  m and do not show large differences in  $\text{O}_2$  fluxes under light and dark conditions (left side of each panel). In contrast, sites 4, 5, and 6 are at water depths between 1 m and 2.5 m and show large differences in  $\text{O}_2$  fluxes under light and dark conditions, providing evidence for benthic photosynthesis (right side of each panel).

highly variable and range from 4% (site 2) to 48% (site 8). Calculating  $\text{N}_2$  production efficiencies based on N fluxes offers the advantage of avoiding assumed C : N ratios of the decomposing organic matter, as required in alternative

approaches (e.g., Ibarra-Obando et al. 2004). In the case of St. Georges Basin, C : N ratios are 21 and 42 at silty to sandy sites 6 (71% porosity) and 7 (61% porosity), respectively, and range from 12 to 16 at muddy sites (with

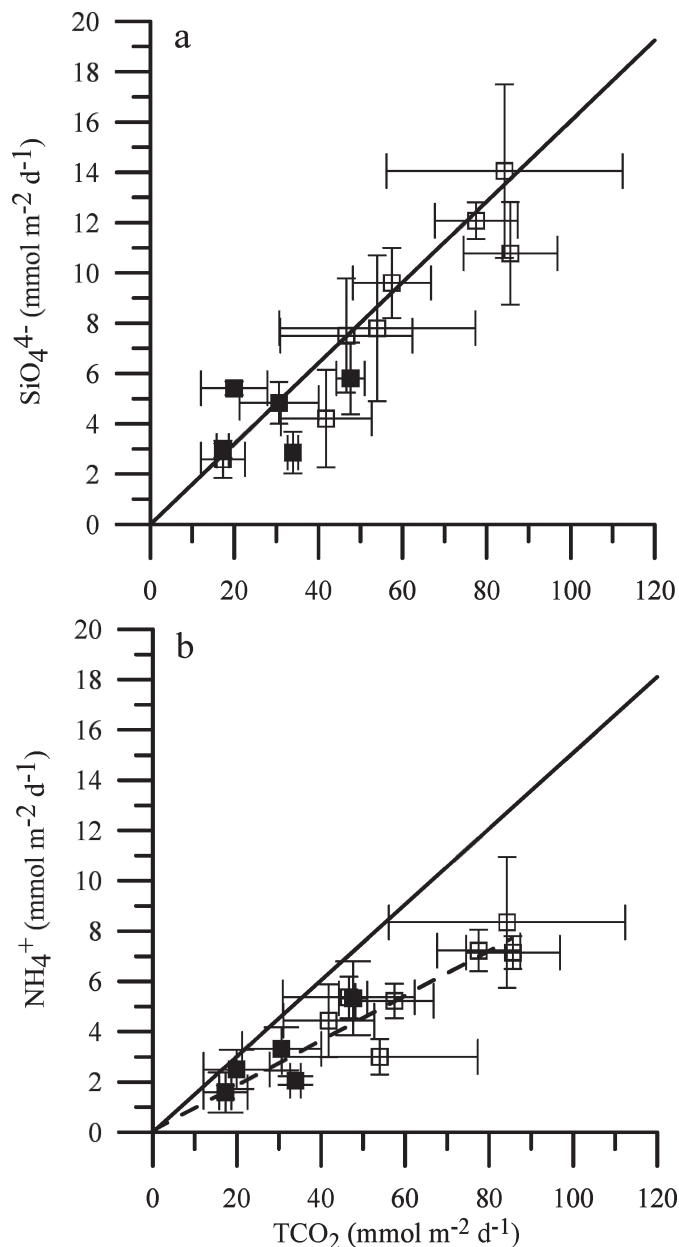


Fig. 4. Cross plots of (a)  $\text{TCO}_2$  versus Si and (b)  $\text{TCO}_2$  versus  $\text{NH}_4^+$  benthic fluxes under dark conditions, derived from in situ benthic chamber (open squares) and core (filled squares) incubations. Error bars represent the deviation from the average. (a) Solid line represents C:Si ratio found in diatoms (Brezekinski 1985). (b) Solid line represents C:N ratio according to Redfield (6.6); dashed line represents linear regression through all data, giving a slope of 11.

86% to 93% porosities), demonstrating that C:N ratios of the bulk organic matter generally exceed the Redfield ratio of 6.6 determined on fresh marine organic matter. As an alternative to the proposed use of the  $\text{N-N}_2$ :DIN benthic flux ratio as a measure for net N removal from the system, one may consider using the benthic  $\text{N-N}_2$ :TN flux ratio, with  $\text{TN} = \text{TIN} + \text{dissolved organic nitrogen (DON)}$ , as it accounts for the DON flux. Benthic DON fluxes have been

shown to be large in some cases and to be spatially and temporarily highly variable (Tyler et al. 2003; Sundbäck et al. 2004; Eyre and Ferguson 2005), but it remains largely unknown to what degree the DON produced in sediments is bioavailable in the water column (Eyre and Ferguson 2005).

*Coupling of C and Si mobilization*—Average  $\text{TCO}_2$ :Si benthic flux ratios derived from benthic chamber ( $7.0 \pm 1.0$ ) and core incubation ( $7.2 \pm 2.3$ ) experiments under dark conditions are very close to the average composition of diatoms (6.2). Independently, pore-water modelling results indicate that depth-dependent rates of C and Si mobilization are one order of magnitude higher in the top 0.5 cm, as compared to underlying sediments, and that C:Si production rate ratios in the top 0.5 cm are very close to the average composition of diatoms. Results from the calculation of production rates may potentially bear some uncertainty, because the derived polynomial fit function is sometimes only based on a few data points and the bioenhanced flux factor is estimated from published data. However, the general consistency in the calculated data set (Table 2) argues against significant errors caused by the fitting procedure to few data points, and deviations from the estimated bioenhanced flux factor would not change the pattern of vertical production rates and  $\text{TCO}_2$ :Si production rate ratios.

The observations of a distinct C:Si benthic flux ratio and the very high mineralization rates for both constituents in the uppermost 0.5 cm, as compared to those of underlying sediments, have important implications. The C:Si benthic flux ratio directly points to diatoms delivering a highly labile organic matter fraction to surface sediments and further indicates congruent mobilization of C and Si from diatoms. Only recently it was discovered that diatoms preferentially sink to the sediment and may supply 100% of the biomass to coastal sediments, although the phytoplankton in the study was flagellate dominated (Waite et al. 2005). In this study, evidence is given that labile organic matter and associated biogenic silica in surface sediments are derived from benthic and pelagic biomass (see *Basin-wide C, N, and P budgets*). Given the microbial control of C mobilization and the chemical control of Si mobilization in sediments, what leads to a coupling of the Si and C mobilization rates?

The siliceous diatom frustule is typically very delicate and has a very high specific surface area. During the lifetime and immediately after starvation of the diatom cell the siliceous frustule is encapsulated by a dissolved organic matter layer primarily consisting of carbohydrates and amino acids, referred to as extracellular polymeric substances (Hoagland et al. 1993). As carbohydrates and amino acids are prime carbon sources for bacteria, extracellular polymeric substances decompose rapidly and contribute significantly to respiration in the water column (Kepkay 1994; Mari 1999). The C:N ratio of extracellular polymeric substances has been shown to be variable and is likely coupled to the ambient nutrient status. A C:N ratio close to the Redfield ratio has been found under nutrient-replete conditions (Biddanda and Benner 1997; Mari 1999),

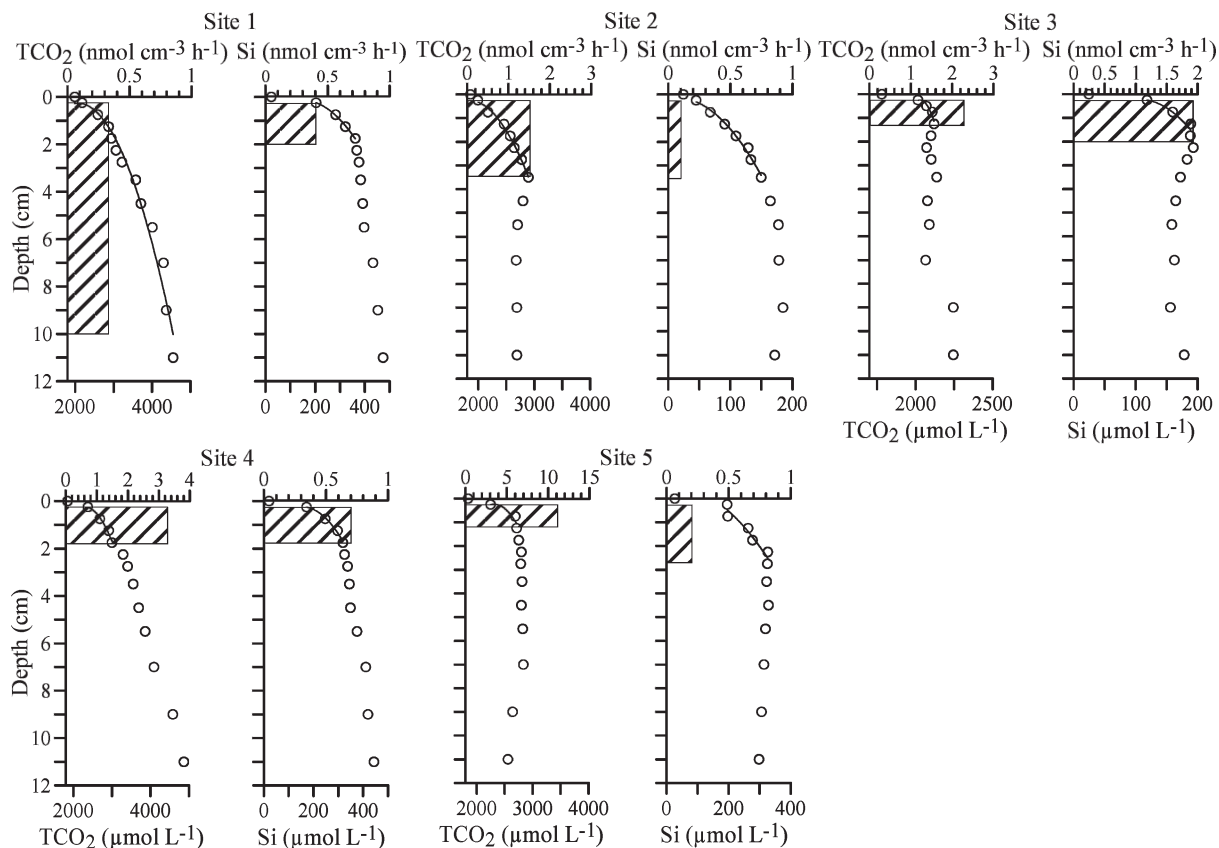


Fig. 5.  $\text{TCO}_2$  and Si pore-water profiles for sites 1 to 5 with the calculated depth-dependent rates of production (hatched bars). The curved lines represent the polynomial fits, which were used to calculate production rates. For calculation procedures, see *Methods and materials*. Note differences in scale on x-axis.

whereas C:N ratios of up to 12 were found in extracellular polymeric substances formed by planktonic diatoms under N-depleted conditions (Engel et al. 2002) and C:N ratios of up to 40 were inferred for extracellular polymeric

Table 2. Modelled production rates of total dissolved inorganic carbon ( $\text{TCO}_2$ ) and silica (Si) below 0.5 cm,  $R_{>0.5}\text{-TCO}_2$  and  $R_{>0.5}\text{-Si}$  (Fig. 5); between 0 and 0.5 cm,  $R_{0-0.5}\text{-TCO}_2$  and  $R_{0-0.5}\text{-Si}$ ; and the ratios of  $\text{TCO}_2$ :Si production rates between 0 and 0.5 cm in sediment depth,  $\text{TCO}_2$ : $\text{Si}_{0-0.5}$ . All production rates are given in  $\text{nmol cm}^{-3} \text{h}^{-1}$ . Production rates were derived from pore-water profiles and do not account for bioirrigation. When depth-integrated rates are multiplied with a bioenhanced flux factor, the calculated rates match measured average total benthic fluxes (see text).  $\text{TCO}_2$  and Si production rates are typically an order of magnitude higher in the top 0.5 cm compared to the depth interval below. The ratios of  $\text{TCO}_2$ :Si production rates within the top interval are close to the average carbon (C):Si molar ratio of diatoms (6.2).

Site	$\text{TCO}_2$ :				$\text{Si}_{0-0.5}$
	$R_{>0.5}\text{-TCO}_2$	$R_{0-0.5}\text{-TCO}_2$	$R_{>0.5}\text{-Si}$	$R_{0-0.5}\text{-Si}$	
1	0.34	20.52	0.38	2.96	6.93
2	1.45	34.41	0.09	4.36	7.89
3	2.24	22.27	1.89	3.61	6.18
4	3.35	32.60	0.70	5.33	6.12
5	12.13	26.24	0.19	4.74	5.54

substances formed by microphytobenthos (Cook et al. 2004).

We hypothesize that diatom-encapsulating extracellular polymeric substances represent the most labile organic fraction in surface sediment and that continued decomposition of the extracellular polymeric substances layer exposes the siliceous frustule to Si-undersaturated seawater, which in turn gives rise to Si dissolution. Under these conditions, the Si dissolution rate must be limited by the extracellular polymeric substances decomposition rate. Therefore, the rates of the two processes are coupled, and congruent mobilization of C and Si is observed. The reasoning for our observation is supported by a study on biogenic silica dissolution in deep-sea environments (Van Cappellen et al. 2002). This study showed that the theoretical Si mineralization rate in surface water exceeds measured rates, and it was concluded that the organic coating (i.e., the layer of extracellular polymeric substances) inhibits biogenic Si dissolution during an early phase of diatom mineralization. The presence of a very small but highly labile organic matter fraction in the top sediment was also recently observed elsewhere (Canavan et al. 2006). In the study of Canavan et al. the most labile fraction was less than 7% of the bulk organic matter fraction but contributed about 85% of the total organic matter degradation rate; the depth-dependent carbon degradation rates exceeded those derived in this study

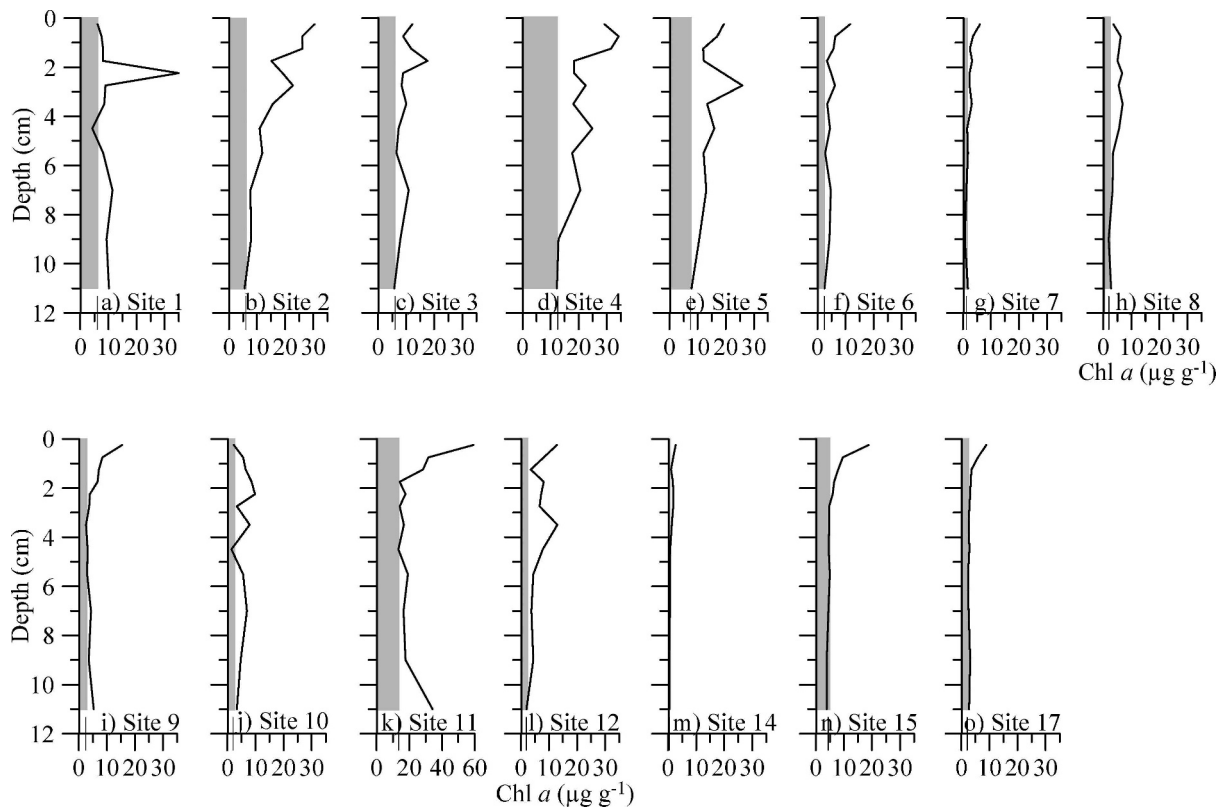


Fig. 6. (a–o) Chlorophyll *a* (Chl *a*) depth profiles. The gray shading represents background concentrations, which are used to calculate excess Chl *a* inventories (= total – background). All x-axes have the same scale except for site 11 (k).

and were largely restricted to the zone of oxic respiration and denitrification.

**Basin-wide C, N, and P budgets**—Catchment load data can be converted to mean basin fluxes (e.g., the given sediment load [ $5.4 \times 10^6 \text{ kg yr}^{-1}$ ] of St. Georges Basin equals a sedimentation rate of  $0.03 \text{ cm yr}^{-1}$ , assuming

a grain density of  $2.65 \text{ g cm}^{-3}$  and a porosity of 80%). Given an average organic carbon concentration of 7 wt%, representative for muddy sites, an organic carbon burial rate of  $1.9 \text{ mmol m}^{-2} \text{ d}^{-1}$  is calculated. Because the organic carbon burial rate is quantitatively negligible compared to the measured  $\text{TCO}_2$  benthic fluxes ( $35\text{--}70 \text{ mmol m}^{-2} \text{ d}^{-1}$ ), the rate of carbon deposition and

Table 3. Sediment properties at study sites. TOC, total organic carbon; TN, total nitrogen; C:N, molar carbon (C):nitrogen (N) ratio; n.a., not applicable. Chlorophyll *a* (Chl *a*) inventories and organic C deposition ( $C_{\text{dep}}$ ) rates are calculated with a mass balance approach (see *Materials and methods for details*). Minimum and maximum carbon deposition rates were calculated using a C:Chl *a* ratio of 50 and 75 (wt:wt).

Site	Water depth (m)	Chl <i>a</i> ( $\mu\text{g cm}^{-2}$ )	$C_{\text{dep}}$ ( $\text{mmol m}^{-2} \text{ d}^{-1}$ )	Porosity	TOC (wt%)	TN (wt%)	C:N
12	0.9	14.4	45–68	n.a.	n.a.	n.a.	n.a.
6	1.1	11.9	37–55	0.71	1.79	0.10	20.88
7	1.5	10.1	32–47	0.60	1.09	0.03	42.39
2	1.6	17.6	55–82	0.92	8.08	0.75	12.65
3	1.6	16.0	50–75	0.86	5.50	0.41	15.57
4	2	25.5	80–120	0.91	10.46	0.90	13.58
5	2.2	22.3	70–105	0.88	7.82	0.69	13.27
15	4.7	4.7	15–22	n.a.	n.a.	n.a.	n.a.
14	5	7.5	24–35	n.a.	n.a.	n.a.	n.a.
17	5.7	6.6	21–31	n.a.	n.a.	n.a.	n.a.
8	8.1	10.8	38–51	0.82	2.88	0.21	16.00
9	8.1	6.1	19–29	n.a.	n.a.	n.a.	n.a.
11	8.4	7.0	22–33	n.a.	n.a.	n.a.	n.a.
10	9	12.1	38–57	n.a.	n.a.	n.a.	n.a.
1	9.8	6.8	21–32	0.91	7.37	0.72	12.02

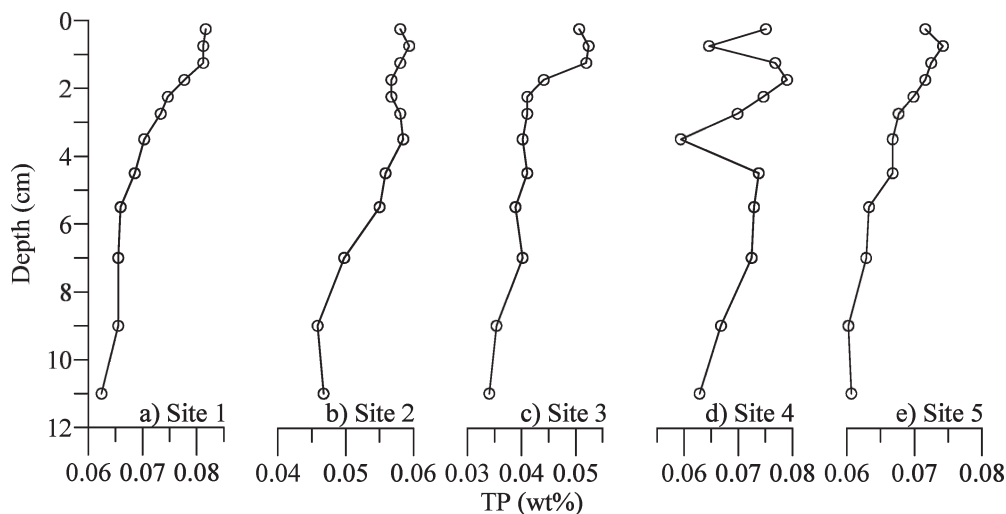


Fig. 7. (a–e) Depth profiles of total phosphorus (TP) in sediments. Except for site 4 all sites exhibit a distinct TP enrichment in surface sediments, indicating that a significant fraction of mobilized P is scavenged by particles. Note differences in scales on x-axis.

decomposition should be similar under steady-state conditions. This condition is tested by comparing the carbon deposition rate derived from sediment Chl *a* inventories ( $n = 16$ ) with the average  $\text{TCO}_2$  benthic fluxes measured in benthic chambers under dark conditions ( $n = 8$ ). C deposition and flux data are pooled into groups according to the depth ranges from which they originate (0–2.5, 4–6, 8–10 m; Fig. 8). A very good agreement is found between the two approaches; however, a distinct difference between the carbon depositional flux at shallow and deep sites is observed (Fig. 8). At sites with a water depth between 0 m and 3 m, the average C depositional flux is  $60 \text{ mmol C m}^{-2} \text{ d}^{-1}$ , whereas at depths between 4–6 m and 8–10 m,

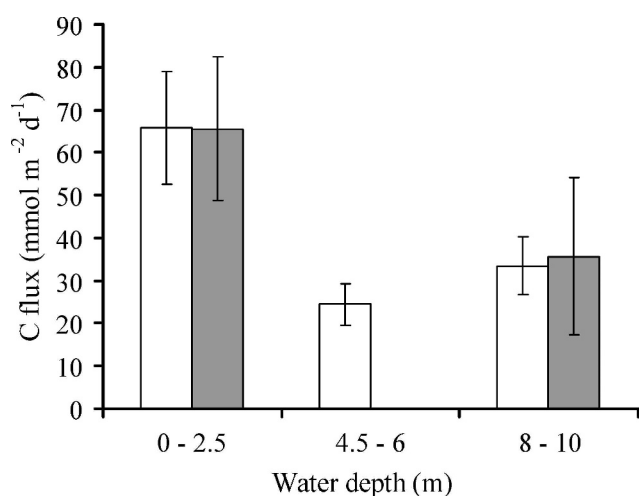


Fig. 8. Comparison of estimated organic carbon flux to the sediment (open bars) to average in situ  $\text{TCO}_2$  benthic fluxes under dark conditions (gray bars). No benthic flux data exist for the water depth interval from 4.5 m to 6 m. Error bars on organic carbon flux columns represent the range of fluxes resulting from C:chlorophyll *a* (Chl *a*) ratios (wt:wt) of 50 and 75. Error bars on benthic  $\text{TCO}_2$  flux columns represent deviations from the average.

the C depositional flux is 25 and  $35 \text{ mmol m}^{-2} \text{ d}^{-1}$ , respectively.

For several reasons, we attribute the higher C deposition rate at water depths of less than 3 m to the growth of microbenthic algae in shallow areas. At water depths shallower than 3 m, the daily average PAR flux was found to be higher than  $90 \mu\text{mol m}^{-2} \text{ s}^{-1}$  (Table 1), and differences in  $\text{TCO}_2$  and  $\text{O}_2$  fluxes between light and dark chambers indicate benthic photosynthesis under light conditions at sites 4, 5, and 6. In contrast, at water depths below 3 m the daily average PAR was less than  $30 \mu\text{mol m}^{-2} \text{ s}^{-1}$ , and no discernable differences in benthic fluxes between light and dark chambers were observed. Furthermore, as Chl *a* concentrations in the surface water were similar in shallow and deep areas, water column primary production appears to be constant regardless of the water depth, and a higher carbon flux through the water column in shallow areas is unlikely.

Similar to the basin-wide C budget, N and P inputs to the sediment can be quantitatively compared to benthic and burial N and P fluxes to identify major sedimentary processes affecting the nutrient status in the water column. The given catchment N load ( $139 \times 10^3 \text{ kg yr}^{-1}$ ) equals a basin-wide external input of  $0.66 \text{ mmol m}^{-2} \text{ d}^{-1}$  which compares reasonably with the loss of N by net  $\text{N-N}_2$  production of  $1 \pm 0.9$  plus the N burial rate of  $0.15 \text{ mmol m}^{-2} \text{ d}^{-1}$ . The latter is calculated using an average TN concentration of 0.5 wt% and the same sedimentation rate, grain density, and porosity as are used for the C burial rate (see above). Importantly, the external N input ( $\sim 0.5\text{--}1.2 \text{ mmol m}^{-2} \text{ d}^{-1}$ ) is only a fraction of the total N input to the sediment (i.e., the sum of the benthic TIN flux and N burial [ $6.6 \pm 3.3 \text{ mmol m}^{-2} \text{ d}^{-1}$ ]), demonstrating the importance of N cycling within the coastal lagoon. Every N atom will pass through the surface sediment and reenter the water column five to 13 times before it will get lost from the N cycle through  $\text{N}_2$

production or N burial. In the case of P, the removal efficiency is much higher. The benthic  $\text{PO}_4^{3-}$  flux ( $0.005 \pm 0.005 \text{ mmol m}^{-2} \text{ d}^{-1}$ ) is similar in magnitude to the loss of P through burial ( $0.008 \text{ mmol m}^{-2} \text{ d}^{-1}$ ). P burial is calculated in a fashion analogous to that of TN, but using a TP concentration of 0.06 wt%. Given similar proportions of P being reintroduced to the water column and P being buried, every P atom passes twice, on average, through the benthic–pelagic loop before it becomes buried. Differences in N and P removal from the internal nutrient cycles are discussed below.

*Nutrient cycles and primary production*—DIN and DIP concentrations are very low in the main basin, with DIN and DIP concentrations typically in the range of 0.6–2 and 0.02–0.04  $\mu\text{mol L}^{-1}$ , respectively. In contrast, Si levels are consistently high, with concentrations above 35  $\mu\text{mol L}^{-1}$ . Based on laboratory experiments and field observations, critical nutrient ratios in combination with nutrient concentrations have been derived and used to assess the likely nutrient limitation of primary production in coastal waters (e.g., Dortch and Whitledge [1992], and references herein; Justić et al. 1995). More recently, the same conclusions were drawn when the nutrient status approach was compared to bioassays (Fujiki et al. 2004). In this study, the observed DIP concentrations in surface water are consistently below 0.1  $\mu\text{mol L}^{-1}$ , and DIN:DIP ratios range between 22 and 30 at three sites (sites 8, 10, 13) and exceed 30 at 6 sites (sites 6, 9, 11, 12, 15, and 17). Only one site had a DIN:DIP ratio slightly below 22 (site 14: 19). P limitation was indicated at DIP concentrations of  $<0.2 \mu\text{mol L}^{-1}$  (Dortch and Whitledge 1992; Fujiki et al. 2004) and at concentrations of  $<0.1 \mu\text{mol L}^{-1}$  (Justić et al. 1995). Therefore, P limitation is indicated based on DIP concentrations throughout the main basin and in Erowal Bay regardless of which threshold value is used. DIN:DIP ratios of  $>20$  (Fujiki et al. 2004),  $>22$  (Justić et al. 1995), and  $\geq 30$  (Dortch and Whitledge 1992) have been used as a second criteria for P limitation. Since six out of 10 sites exceed a ratio of 30 and another three sites exceed a ratio of 22, the DIN:DIP ratio additionally indicates P limitation for primary production. P-limited primary production has been proposed as an indicator for more pristine coastal environments (Howarth et al. 1995; Smith 2006).

The low nutrient and Chl *a* levels indicate overall oligotrophic conditions. Low-nutrient conditions favor the dominance of picophytoplankton over microphytoplankton, as smaller cells acquire and use nutrients more efficiently than larger cells (Raven 1998). Following this pattern, the high proportion of typically small-sized cyanophytes found in St. Georges Basin complies with the concurrent nutrient status. Low levels of Chl *a*, P-limited primary production, and the likely dominance of small-sized phytoplankton consistently indicate that St. Georges Basin has retained its oligotrophic, more pristine character until the present time.

Despite the dominance of cyanophytes and a large proportion of green flagellates in the phytoplankton community, C:Si benthic flux ratios and modelled C and Si mobilization rates using pore-water profiles provide

evidence that the labile organic matter settling to the sediment is derived from diatoms (*see above*). Note that this observation is made regardless of the water depth and, therefore, regardless of a possible influence by microphytobenthos. Preferential settling of diatoms to the sediment implies an important fractionation of phytoplankton biomass. Biomass fractionation due to preferential sinking of diatoms is well known in deep-sea environments (e.g., Dugdale and Wilkerson 1998) and has more recently been observed in a coastal setting during a phytoplankton bloom (Waite et al. 2005). The latter study found the total biomass flux to the sediment to be made up by diatoms, despite phytoplankton dominance by flagellates. As a consequence of the preferential removal of diatoms from the production–remineralization loop in the water column, only diatoms contributed to the new production. By analogy, export and new production are also likely to be driven by diatoms in the oligotrophic and shallow-water environment of St. Georges Basin.

The rapid sinking of diatoms to the sediment, as opposed to the longer residence time and more intense mineralization of other dead phytoplankton biomass in the water column, has implications for N and P cycles within the lagoon. Only when organic matter is mineralized under suboxic conditions, as found in surface sediments, is the mobilized N (partially) transformed into  $\text{N}_2$  (*see above*), which is no longer bioavailable, except for microbial N-fixation. Similarly, but to a much larger extent, P is removed from the bioavailable pool by adsorption to and co-precipitation of iron(oxy)hydroxides in surface sediments, if the bottom water is oxic and sufficient reactive iron is supplied to the sediments. In other words, rapid sinking and mineralization of diatoms in surface sediments is an effective mechanism to remove bioavailable N and P. The higher degree of P removal relative to N is reflected in the observed DIN:DIP benthic flux ratios in the range of 290 to 900, as opposed to the ratio of 16 found in marine phytoplankton. Particularly when the water residence time is long and the basin is shallow one can expect water column nutrient ratios to reflect the fractionation of N and P when leaving the sediment. Indeed, the highest DIN:DIP ratio in the water column is found in Erowal Bay (site 12: 242), a shallow ( $<1.5\text{-m}$ ) basin in the northeast portion of the main basin of St. Georges Basin that has very restricted water exchange as a result of the buildup of a sandbar. The second highest DIN:DIP ratio is found at a water depth of 1.1 m (site 6: 122), if sites under brackish water influence (sites 7 and 16) are excluded. In conclusion, diatoms induce a mechanism to remove P more efficiently than N from the bioavailable pool, resulting in low DIP concentrations and, possibly, overall P limitation. This finding is likely to be particularly important for the nutrient limitation in shallow lagoons with long water residence time.

In the case of increasing nutrient loads from the catchment, the described mechanism controlling the present-day benthic–pelagic coupling and nutrient availability may change. TN and TP loads to St. Georges Basin are projected to increase by a factor of 2 to 3 as a result of enhanced land use and urbanization (Shoalhaven City Council pers. comm.). As a consequence, an enhanced flux

of biomass to the sediment and higher rates of organic matter mineralization are expected, which will induce higher benthic oxygen consumption. Vertical mixing of the water column may no longer be sufficient throughout the year to compensate the enhanced oxygen consumption in the deeper parts of the basin. Temporary bottom-water suboxia would significantly affect the magnitude and ratio of benthic nutrient and gas fluxes, as denitrification and efficient  $\text{PO}_4^{3-}$  adsorption to iron(oxy)hydroxides would cease. The induced higher benthic nutrient fluxes would trigger biogeochemical changes in the water column, commonly associated with eutrophication, including higher primary production, changes in nutrient ratios, and changes in the phytoplankton community.

### References

- BERELSON, W. M., D. T. HEGGIE, A. LONGMORE, T. KILGORE, G. NICHOLSON, AND G. SKYRING. 1998. Benthic nutrient recycling in Port Phillip Bay, Australia. *Estuar. Coast. Shelf Sci.* **46**: 917–934.
- BIDDANDA, B., AND R. BENNER. 1997. Carbon, nitrogen, and carbohydrate fluxes during the production of particulate and dissolved organic matter by marine phytoplankton. *Limnol. Oceanogr.* **42**: 506–518.
- BOON, R. J., AND G. C. A. DUINEVELD. 1998. Chlorophyll *a* as a marker for bioturbation and carbon flux in southern and central North Sea sediments. *Mar. Ecol. Prog. Ser.* **162**: 33–43.
- BREZINSKI, M. A. 1985. The Si:C:N ratio of marine diatoms: Interspecific variability and the effect of some environmental variables. *J. Phycol.* **21**: 347–357.
- CANAVAN, R. W., C. P. SOMP, P. JOURABCHI, P. VAN CAPPELLEN, A. M. LAVERMAN, AND G. A. VAN DEN BERG. 2006. Organic matter mineralization in sediment of a coastal freshwater lake and response to salinization. *Geochim. Cosmochim. Acta* **70**: 2836–2855.
- COOK, P. L. M., A. T. REVILL, E. C. V. BUTLER, AND B. D. EYRE. 2004. Carbon and nitrogen cycling on intertidal mudflats of a temperate Australian estuary. II. Nitrogen cycling. *Mar. Ecol. Prog. Ser.* **280**: 39–54.
- DALSGAARD, T. 2003. Benthic primary production and nutrient cycling in sediments with benthic microalgae and transient accumulation of macroalgae. *Limnol. Oceanogr.* **48**: 2138–2150.
- DORTCH, Q., AND T. E. WHITLEDGE. 1992. Does nitrogen or silicon limit phytoplankton production in the Mississippi River plume and nearby regions? *Cont. Shelf Res.* **12**: 1293–1309.
- DUGDALE, R. C., AND F. P. WILKERSON. 1998. Silicate regulation of new production in the equatorial Pacific upwelling. *Nature* **391**: 270–273.
- ENGEL, A., S. GOLDTHWAIT, U. PASSOW, AND A. ALLDREDGE. 2002. Temporal decoupling of carbon and nitrogen dynamics in a mesocosm diatom bloom. *Limnol. Oceanogr.* **47**: 753–761.
- EYRE, B. D., AND A. J. FERGUSON. 2005. Benthic metabolism and nitrogen cycling in a subtropical east Australian estuary (Brunswick): Temporal variability and controlling factors. *Limnol. Oceanogr.* **50**: 81–96.
- , S. RYSGAARD, T. DALSGAARD, AND P. B. CHRISTENSEN. 2002. Comparison of isotope pairing and  $\text{N}_2$ :Ar methods for measuring sediment denitrification—assumptions, modifications, implications. *Estuaries* **25**: 1077–1087.
- FORSTER, S., G. N. GLUD, J. K. GUNDERSEN, AND M. HUETTLE. 1999. In situ study of bromide tracer and oxygen flux in coastal sediments. *Estuar. Coast. Shelf Sci.* **49**: 813–827.
- FRY, B., W. BRAND, F. J. MERSCH, K. THOLKE, AND R. GARRITT. 1992. Automated analysis system for  $\delta^{13}\text{C}$  and  $\delta^{15}\text{N}$  measurement. *Anal. Chem.* **64**: 288–291.
- FUJIKI, T., T. TODA, T. KIKUCHI, H. AONO, AND S. TAGUCHI. 2004. Phosphorous limitation of primary productivity during the spring-summer blooms in Sagami Bay, Japan. *Mar. Ecol. Prog. Ser.* **283**: 29–38.
- GLUD, R. N., J. K. GUNDERSEN, H. RØY, AND B. B. JØRGENSEN. 2003. Seasonal dynamics of benthic  $\text{O}_2$  uptake in a semi-enclosed bay: Importance of diffusion and faunal activity. *Limnol. Oceanogr.* **48**: 1265–1276.
- GRASSHOFF, K., M. EHRHARDT, AND K. KREMLING. 1983. Methods of seawater analysis. Verlag Chemie.
- HAGY, J. D. III, W. R. BOYNTON, AND D. A. JASINSKI. 2005. Modelling phytoplankton deposition to Chesapeake Bay sediments during winter-spring: Interannual variability in relation to river flow. *Estuar. Coast. Shelf Sci.* **62**: 25–40.
- HALL, P. O. J., AND R. C. ALLER. 1992. Rapid, small-volume, flow injection analysis for  $\Sigma\text{CO}_2$  and  $\text{NH}_4^+$  in marine and freshwaters. *Limnol. Oceanogr.* **37**: 1113–1119.
- HAMMOND, D. E., K. M. CUMMINS, J. MC MANUS, W. M. BERELSON, G. SMITH, AND F. SPAGNOLI. 2004. Methods for measuring benthic nutrient flux on the California Margin: Comparing shipboard core incubations to in situ lander results. *Limnol. Oceanogr. Methods* **2**: 146–159.
- HOAGLAND, K. D., J. R. ROSOWSKI, M. R. GRETZ, AND S. C. ROEMER. 1993. Diatom extracellular polymeric substances: Function, fine structure, chemistry, and physiology. *J. Phycol.* **29**: 537–566.
- HOWARTH, R. W., H. S. JENSEN, R. MARINO, AND H. POSTMA. 1995. Transport to and processing of P in near-shore and oceanic waters, p. 323–345. *In* H. Tiessen [ed.], Phosphorous in the global environment. Wiley.
- , R. MARINO, AND D. SCAVIA. 2003. Priority topics for nutrient pollution in coastal waters: An integrated national research program for the United States. National Centers for Coastal Ocean Science, National Ocean Service, National Oceanic and Atmospheric Administration.
- HULTH, S., AND OTHERS. 2005. Nitrogen removal in marine environments: Recent findings and future research challenges. *Mar. Chem.* **94**: 125–145.
- IBARRA-OBANDO, S. E., S. V. SMITH, M. POUMIAN-TAPIA, V. CAMACHO-IBAR, J. CARRIQUIRY, AND M. MONTES-HUGO. 2004. Benthic metabolism in San Quintin Bay, Baja California, Mexico. *Mar. Ecol. Prog. Ser.* **283**: 99–112.
- JEFFREY, S. W., AND M. VESK. 1997. Introduction to marine phytoplankton and their pigment signatures, p. 407–428. *In* S. W. Jeffrey, R. F. C. Mantoura and S. W. Wright [eds.], Phytoplankton pigments in oceanography. United Nations Education, Science and Cultural Organization (Paris).
- , AND S. W. WRIGHT. 2006. Photosynthetic pigments in marine microalgae: Insights from cultures and the sea, p. 39–90. *In* D. V. Subba Rao [ed.], Algal cultures, analogues of blooms and applications. Science Publishers.
- JØRGENSEN, B. B., AND K. RICHARDSON. 1996. Eutrophication in coastal marine ecosystems. *Coastal and Estuarine Studies* **52**. American Geophysical Union.
- JUSTIĆ, D., N. N. RABALAIS, R. E. TURNER, AND Q. DORTCH. 1995. Changes in nutrient structure of river-dominated coastal waters: Stoichiometric nutrient balance and its consequences. *Estuar. Coast. Shelf Sci.* **40**: 339–356.
- KANA, T. M., M. DARKANGELO, M. D. HUNT, J. B. OLDHAM, G. E. BENNETT, AND J. C. CORNWELL. 1994. Membrane inlet mass spectrometer for rapid high-precision determination of  $\text{N}_2$ ,  $\text{O}_2$ , and Ar in environmental water samples. *Anal. Chem.* **66**: 4166–4170.

- KEPKAY, P. E. 1994. Particle aggregation and biological reactivity of colloids. *Mar. Ecol. Prog. Ser.* **109**: 293–304.
- KIRK, J. T. O. 1994. Light and photosynthesis in aquatic ecosystems. 2nd ed. Cambridge Univ. Press.
- LASSEN, C., N. P. REVSBECH, AND O. PEDERSEN. 1997. Macrophyte development and resuspension regulate the photosynthesis and production of benthic microalgae. *Hydrobiologia* **350**: 1–11.
- LORENZEN, C. J. 1967. Determination of chlorophyll and pheopigments: Spectrophotometric equations. *Limnol. Oceanogr.* **12**: 343–346.
- LUCAS, C. H. 2003. Observations of resuspended diatoms in the turbid tidal edge. *J. Sea Res.* **50**: 301–308.
- MARI, X. 1999. Carbon content and C:N ratio of transparent exopolymeric particles (TEP) produced by bubbling exudates of diatoms. *Mar. Ecol. Prog. Ser.* **183**: 59–71.
- MEEHAN, A. J., R. J. WILLIAMS, AND F. A. WATFORD. 2005. Detecting trends in seagrass abundance using aerial photograph interpretation: Problems arising with the evolution of mapping methods. *Estuaries* **28**: 462–472.
- MEHRBACH, C., C. H. CULBERSON, J. E. HAWLEY, AND R. M. PYTKOWITZ. 1973. Measurement of the apparent dissociation constants of carbonic acid in sea water at atmospheric pressure. *Limnol. Oceanogr.* **18**: 897–907.
- NIXON, S. W. 1995. Coastal marine eutrophication: A definition, social causes, and future concerns. *Ophelia* **41**: 199–219.
- NORRISH, K., AND J. T. HUTTON. 1969. An accurate X-ray spectrographic method for the analysis of a wide range of geological samples. *Geochim. Cosmochim. Acta* **33**: 431–453.
- PEDERSEN, M. F., S. L. NIELSEN, AND G. T. BANTA. 2004. Interactions between vegetation and nutrient dynamics in coastal marine ecosystems: An introduction, p. 1–15. *In* S. L. Nielsen, G. T. Banta and M. F. Pedersen [eds.], *Estuarine nutrient cycling: The influence of primary producers*. Kluwer.
- RAVEN, J. A. 1998. The twelfth Tansley Lecture. Small is beautiful: The picophytoplankton. *Funct. Ecol.* **12**: 503–513.
- REDFIELD, A. C., B. H. KETCHUM, AND F. A. RICHARDS. 1963. The influence of organisms on the composition of sea water, p. 26–79. *In* M. N. Hill [ed.], *The sea*. V. 2. Wiley Interscience.
- RISGAARD-PETERSEN, N. 2003. Coupled nitrification-denitrification in autotrophic and heterotrophic estuarine sediments: On the influence of benthic microalgae. *Limnol. Oceanogr.* **48**: 93–105.
- SCHULZ, H. D. 2006. Quantification of early diagenesis: Dissolved constituents in pore water and signals in the solid phase, p. 73–124. *In* H. D. Schulz and M. Zabel [eds.], *Marine geochemistry*. Springer-Verlag.
- SHAFFER, G. P., AND M. J. SULLIVAN. 1988. Water column productivity attributable to displaced benthic diatoms in well-mixed shallow estuaries. *J. Phycol.* **24**: 132–140.
- SLOMP, C. P., S. J. VAN DER GAST, AND W. VAN RAAPHORST. 1996. Phosphorous binding by poorly crystalline iron oxides in North Sea sediments. *Mar. Chem.* **52**: 55–73.
- SMETACEK, V. S. 1985. The role of sinking in diatom life-history cycles: Ecological, evolutionary and geological significance. *Mar. Biol.* **84**: 239–251.
- SMITH, V. H. 2006. Response of estuarine and coastal marine phytoplankton to nitrogen and phosphorous enrichment. *Limnol. Oceanogr.* **51**: 3377–3384.
- , S. B. JOYE, AND R. W. HOWARTH. 2006. Eutrophication of freshwater and marine ecosystems. *Limnol. Oceanogr.* **51**: 351–355.
- SUN, M.-Y., R. C. ALLER, AND C. LEE. 1994. Spatial and temporal distributions of sedimentary chloropigments as indicators of benthic processes in Long Island Sound. *J. Mar. Res.* **52**: 149–176.
- , C. LEE, AND R. C. ALLER. 1993. Laboratory studies of oxic and anoxic degradation of chlorophyll-*a* in Long Island Sound sediments. *Geochim. Cosmochim. Acta* **57**: 147–157.
- SUNDBÄCK, K., F. LINARES, F. LARSEN, A. WULFF, AND A. ENGELSEN. 2004. Benthic nitrogen fluxes along a depth gradient in a microtidal fjord: The role of denitrification and microphytobenthos. *Limnol. Oceanogr.* **49**: 1095–1107.
- TYLER, A. C., K. J. MCGLATHERY, AND I. ANDERSON. 2003. Benthic algae control sediment-water column fluxes of organic and inorganic nitrogen compounds in a temperate lagoon. *Limnol. Oceanogr.* **48**: 2125–2137.
- UNDERWOOD, G. J. C., AND J. KROMKAMP. 1999. Primary production by phytoplankton and microphytobenthos in estuaries. *Adv. Ecol. Res.* **29**: 93–153.
- VAN CAPPELLEN, P., S. DIXIT, AND J. VAN BEUSEKOM. 2002. Biogenic silica dissolution in the oceans: Reconciling experimental and field-based dissolution rates. *Glob. Biogeochem. Cycles* **16**: 1075. doi:10.1029/2001GB001431.
- VAN DER BORGH, J.-P., AND G. BILLEN. 1975. Vertical distribution of nitrate concentration in interstitial water of marine sediments with nitrification and denitrification. *Limnol. Oceanogr.* **20**: 953–961.
- WAITE, A. M., Ö. GUSTAFSON, O. LINDAHL, AND P. TISELIUS. 2005. Linking ecosystem dynamics and biogeochemistry: Sinking fractionation of organic carbon in a Swedish fjord. *Limnol. Oceanogr.* **50**: 658–671.
- WENZHÖFER, F., AND R. N. GLUD. 2004. Small-scale spatial and temporal variability in coastal benthic O<sub>2</sub> dynamics: Effects of faunal activity. *Limnol. Oceanogr.* **49**: 1471–1481.

Received: 11 January 2007

Accepted: 18 June 2007

Amended: 16 July 2007